Journal of Materials Chemistry B

ROYAL SOCIETY OF CHEMISTRY

REVIEW

View Article Online
View Journal | View Issue

Cite this: J. Mater. Chem. B, 2023, 11, 3038

Recent developments in carbon dots: a biomedical application perspective

Le Tu,†[ab] Qian Li,†[b] Sheng Qiu,†[a] Meiqin Li,†[b] Jinwoo Shin,†[c] Pan Wu,†[d] Nem Singh,[c] Junrong Li,[b] Qihang Ding,[c] Cong Hu,[e] Xiaoxing Xiong,*[a] Yao Sun*[b] and Jong Seung Kim*[c]

Received 25th December 2022,
Accepted 17th February 2023

DOI: 10.1039/d2tb02794a

rsc.li/materials-b

Recently, newly developed carbon-based nanomaterials known as carbon dots (CDs) have generated significant interest in nanomedicine. However, current knowledge regarding CD research in the biomedical field is still lacking. An overview of the most recent development of CDs in biomedical research is given in this review article. Several crucial CD applications, such as biosensing, bioimaging, cancer therapy, and antibacterial applications, are highlighted. Finally, CD-based biomedicine's challenges and future potential are also highlighted to enrich biomedical researchers' knowledge about the potential of CDs and the need for overcoming various technical obstacles.

1. Introduction

A new era in the family of carbon materials began in 2004[1] with the creation of CDs with fluorescent features during the electrophoretic purification of single-walled carbon nanotubes. The majority of carbon-based nanomaterials are 0D (sizes less than 10 nm, ref. 2) and comprise sp^2 and sp^3 carbon atoms with numerous polymer chains or diverse functional groups bonded to their surfaces.[3] According to their carbon core structure, surface functional groups, and physical characteristics, CDs are categorized as carbon quantum dots (CQDs), carbon nanodots (CNDs), graphene quantum dots (GQDs) as well as carbonized polymer dots (CPDs).[4] CQDs primarily consist of multi-layered graphitic structures and contain a variety of chemical groups that endow them with inherent state luminescence and quantum confinement effects.[5] GQDs are the most differentiated among CDs. GQDs are essentially one or several layers of small graphene fragments that exhibit quantum confinement and edge effects because they have chemical functions on their edge or within an interlayer defect. Electrical conductivity, large surface area, and adjustable PL are some of the additional properties of GQDs.[6] CNDs are highly carbonized nanoparticles that exhibit edge effects but not the quantum confinement effect. Between polymer dots and completely carbonized CDs, CPDs serve as the link since they are crosslinked nanohybrids of carbon and aggregated polymers. Top-down (*e.g.*, laser ablation,[7] arc discharge,[8] or electrochemical oxidation[9]) and bottom-up (*e.g.*, chemical or thermal oxidation,[10] hydrothermal treatment,[11] or microwave[12]) techniques are currently utilized for CD synthesis.

Owing to their tunable photoluminescence, extraordinary physicochemical properties, low cytotoxicity, and exceptional water dispersibility,[16] CDs are presently exhibiting remarkable potential in biosensors,[13] bioimaging,[14] and disease diagnosis/treatment.[15] CDs with diverse biomedical applications, such as optical sensing, bioimaging, chemotherapy, photothermal therapy (PTT), photodynamic therapy (PDT), *etc.*, have been created by strategic design and post-synthetic functionalization. The use of these compact discs in biomedicine is now rapidly growing. The synthesis, PL mechanism, and uses of CDs have all been condensed in a number of review publications. However, the objective of this article is to offer the reader a general understanding of the abundance of carbon dots available for use in the biomedical domain and to aid in determining which design strategy should be chosen to address a particular problem. We have highlighted several essential CD applications, including biosensing, bioimaging, cancer therapy, and antibacterial applications. In order to help shed light on the possible function of CDs in biomedicine, we will also discuss the research trends, future developments, and ongoing debates in this area.

[a] Department of Neurosurgery, The Affiliated Huzhou Hospital, Zhejiang University School of Medicine (Huzhou Central Hospital), Huzhou 313099, P. R. China
[b] Key Laboratory of Pesticides and Chemical Biology, Ministry of Education, College of Chemistry, Central China Normal University, Wuhan 430079, China. E-mail: sunyaogbasp@mail.ccnu.edu.cn
[c] Department of Chemistry, Korea University, Seoul 02841, Korea. E-mail: jongskim@korea.ac.kr
[d] State Key Laboratory of Biocatalysis and Enzyme Engineering, School of Life Sciences, Hubei University, Wuhan 430062, China
[e] Guangxi Key Laboratory of Automatic Detecting Technology and Instruments, Guilin University of Electronic Technology, Guilin 541004, China
† Le Tu, Qian Li, Sheng Qiu, Meiqin Li, Jinwoo Shin, and Pan Wu contributed equally to this work.

2. CDs for biosensing

Timely and accurate *in situ* analysis of the body's abnormal expression of substances is conducive to preventing and treating human diseases. Based on the excellent multiple properties of CDs, including superior photostability, photoluminescence, charge transfer, low toxicity, and good aqueous dispersibility, they have long been used as optical sensor materials in the disciplines of illness diagnosis, food safety analysis, and environmental analysis. In this section, we mainly focus on the precise detection of disease-associated biomarkers.

The accurate detection of disease-associated biomarkers is extremely important in the early identification of diseases. As excellent luminophores, CDs play a vital role in fluorescence-based sensing and electrochemiluminescence sensing for disease-associated biomarkers.[17] To date, CDs have been extensively applied in the field of biomedicine. The dual-signal output strategy avoided false positives and provided higher sensitivity.[18] Hamd-Ghadareh *et al.* constructed RB-conjugated carbon dots (RB-CDs) for ratiometric fluorescence detection of β-amyloid (Aβ) in the presence of gold nanoparticles (AuNPs) as acceptors.[19] Low background, great sensitivity, spatial and temporal controllability, and simple operation are all benefits of electrochemiluminescence (ECL). Therefore, ECL-based CDs hold the inherent advantages of a broad linear range and great selectivity. Recently, boron and nitrogen-codoped carbon dots (BN-CDs) were created by Guo and co-workers as incredibly efficient electrochemiluminescence emitters for the supersensitive detection of HBV-DNA (Fig. 1a).[20] The ECL intensity increased as the HBV-DNA concentration rose (Fig. 1b). The logarithm of the HBV-DNA concentration and ECL intensity has a good linear relationship, as shown in Fig. 1c. The merit of

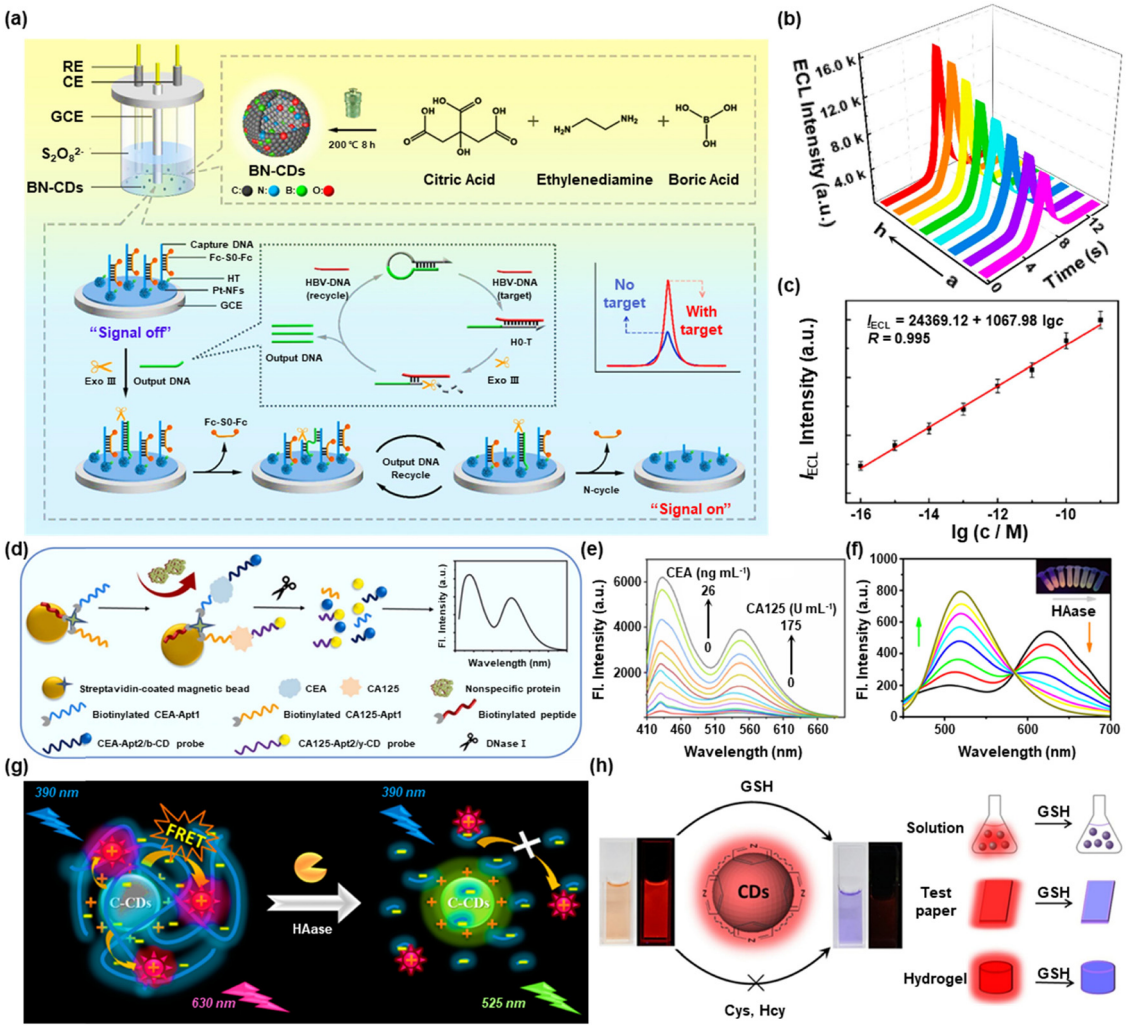

Fig. 1 (a) Schematic illustration of the detection of HBV-DNA based on an Exo III-induced target DNA amplification strategy, (b) ECL response, and (c) calibration curve of HBV-DNA detection. Reproduced with permission.[20] Copyright 2022, American Chemical Society. (d) Process of simultaneous detection of CEA and CA125 and (e) its FL response. Reproduced with permission.[21] Copyright 2022, Elsevier. (f) Fluorescence spectra of C-CDs in response to different doses of HAase. (g) Schematic illustration for the detection of HAase by C-CDs. Reproduced with permission.[22] Copyright 2017, American Chemical Society. (h) Schematic illustration of the visual and accurate detection of GSH according to the color-change and fluorescence-off using p-CDs. Reproduced with permission.[24] Copyright 2020, Elsevier.

tunable wavelengths showed the advantage of CDs in detecting targets simultaneously. Zou *et al.* proposed an MBs/peptides/CD-based stage by employing blue-colored carbon dots (b-CDs) and yellow-colored carbon dots (y-CDs) to simultaneously detect cancer antigen125 (CA125) and carcinoembryonic antigen (CEA) (Fig. 1d).[21] The fluorescence intensity at 430 nm and 550 nm grew simultaneously as more and more CEA and CA125 were administered (Fig. 1e). This platform provided a new perspective for dual or multiple simultaneous detection of tumor makers.

Except for the biomarkers mentioned above, the detection of some biomolecules expressed abnormally also plays a direct or indirect role in the occurrence and progression of the disease. For example, Yang *et al.* designed cationic carbon dots (C-CDs), which were surrounded by a lot of positive charges on the surface to detect HA with high sensitivity (Fig. 1g).[22] As shown in Fig. 1f, the fluorescence intensity at 525 nm increased with the increase of HAase, but the fluorescence intensity at 630 nm dropped. Abnormal GSH levels are commonly associated with diseases such as cancer, HIV, brain mitochondrial damage, and Parkinson's disease.[23] Ultrasensitive and selective identification of GSH expression levels is thus important in biomedicine. For instance, by conducting colorimetric and fluorescent dual modal sensing technologies, Jia *et al.* employed red-emitting CDs (p-CDs) to visually and precisely recognize GSH (Fig. 1h).[24] In biological systems, P-CDs did not respond to other biological thiols, amino acids, and ions. Additionally, p-CDs could monitor GSH visually based on the system's color shift in addition to measuring GSH by a fluorescence test.

3. CDs for bioimaging

Bioimaging technology, a modern and non-invasive research technique, offers limitless potential in the early identification of disease and the direction of lesion therapy. It helps researchers comprehend the tissue structure of organisms and clarify numerous physiological activities. Modern bioimaging approaches include fluorescence imaging (FL), magnetic resonance imaging (MRI), photoacoustic imaging (PAI), and ultrasound imaging (US), *etc.*[25] CDs, as a kind of classical fluorescent probes in the field of fluorescence imaging, are fascinating and vital for guiding the accurate discovery of lesion sites and complete surgical resection. More recently, the preparation of CDs with magnetic properties has attracted much attention and acts as a promising platform for magnetic resonance imaging. In addition, due to the diverse selection of precursors during the preparation process, various imaging modalities could be integrated into a single CD-based platform to exert their advantages respectively.[26] In brief, CDs have been widely exploited in bioimaging and have produced a powerful boosting effect in the biomedical field.

3.1. Fluorescence imaging

Fluorescence imaging, the most promising strategy for *in vivo* precise and non-invasive diagnosis/monitoring, has achieved a satisfactory contribution to basic research and clinical applications. CDs have been proven to have significant potential in fluorescence imaging owing to their intrinsic advantages, including adjustable emission wavelength, high quantum yield, and excellent photostability.[27] In this section, we primarily examine the status and potential future directions of CD-based fluorescence imaging. For instance, a high-performance and selective fluorescence probe for monitoring biological activities *in vivo* was created by Srivastava *et al.* using DNA-conjugated green and red emission CDs (gCD-ssDNA1 and rCD-ssDNA2) (Fig. 2a).[28] As shown in Fig. 2b, when breast cancer cells (MCF-7) were treated with gCD-ssDNA1 or rCD-ssDNA2, their fluorescence was significantly increased in cells in comparison to cells treated with gCD or rCD alone. However, related to the formation of ds-DNA complexes that aggregate when complementary DNA base pairs attached to the individual particles hybridize, fluorescence was reduced in cells treated with a mixture of gCD-ssDNA1 and rCD-ssDNA2 in comparison with those treated with the mixture of gCD and rCD. The fluorescence intensity dropped sharply due to the close proximity of gCD-ssDNA1 and rCD-ssDNA2, which induced the ds-DNA complex to form and resulted in a nonradiative energy transfer process between the two CDs.

Recent literature *via* many studies has shown that organelle damage or dysfunction can lead to significant diseases. Therefore, if the morphological or functional damage of organelles is able to be tracked in real-time, additional compelling evidence for the early identification and treatment of associated disorders can be presented. The development of efficient methods for precise visualization of different organelles using intrinsic or post-modified CDs has shown great significance in the biomedical field. Based on this aim, E. Shuang *et al.* designed four carbon dots (ECDs, NCDs, GCDs, and LCDs) with various surface chemistry and achieved tunable fluorescence imaging of organelles by different uptake mechanisms (Fig. 2c).[29] In addition, the interactions with organelles were rationally explained by exploring the connection between surface chemistry and CDs' capacity for subcellular targeting. These four kinds of CDs were employed to co-incubate with LoVo cells to obtain 3D images of organelles (Fig. 2d). Furthermore, zebrafish was chosen as a model for *in vivo* imaging. The results revealed that all four carbon dots primarily accumulated in the entire body, gut, and vitelline, respectively, suggesting that the produced CDs were able to get beyond the mucus barrier and interplay with the cells of zebrafish. This work provided flexible ideas for designing CDs that specifically target organelles.

Fluorescence imaging can not only illuminate the lesion site but can also be used to distinguish the different states of cells, in which propidium iodide (PI) has long been used to differentiate between living and dead cells in commercial kits. For example, Yu *et al.* fabricated ultrabright sulfur-doped CDs (S-CDs) with excitation wavelength-independent fluorescence emission properties that could be used to distinguish between living and dead cells.[30] Fig. 2e depicts the mechanism of S-CDs to differentiate between live and dead cells. Notable differences between the two cell types' uptake pathways were used to explain this phenomenon. Specifically, functionally and structurally intact

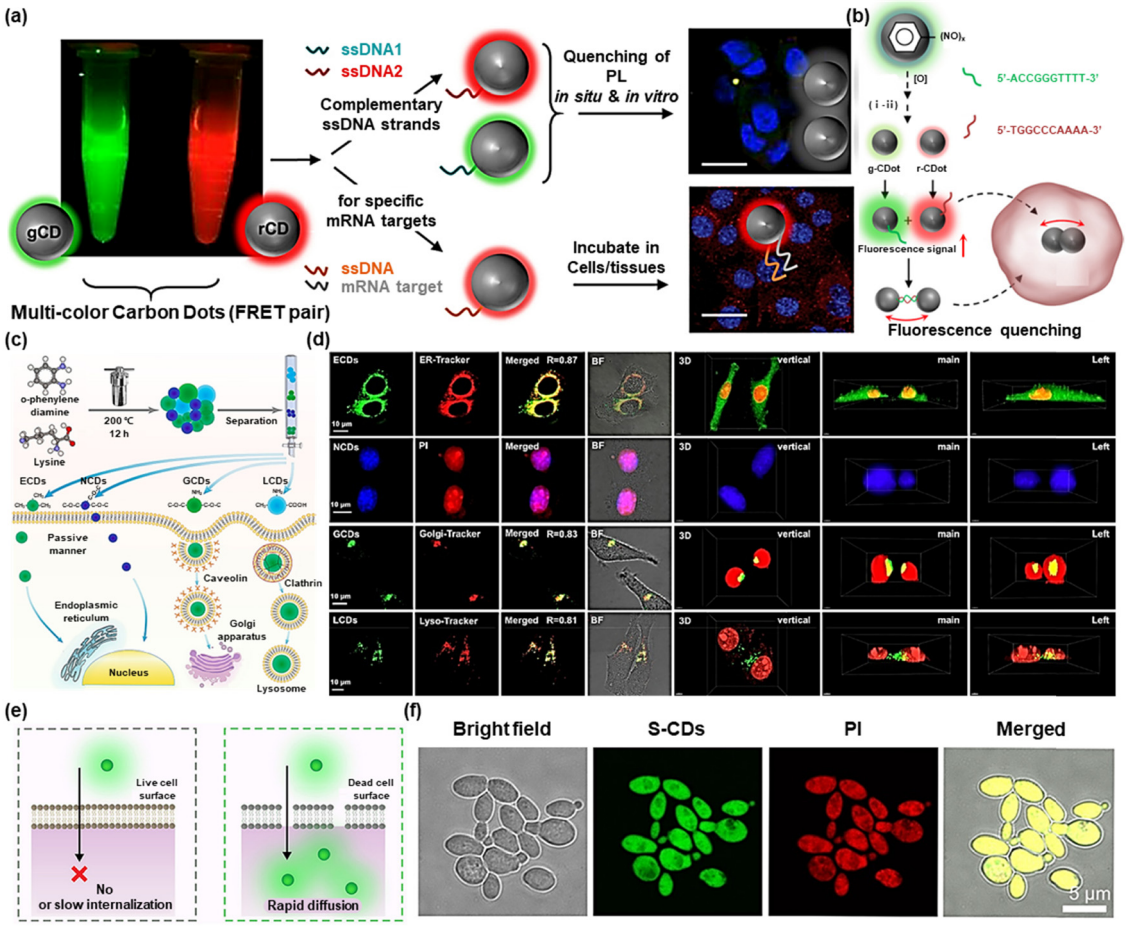

Fig. 2 (a) Schematic illustration of anisotropic complementarity in DNA–DNA hybridization directed assembly. (b) Spontaneous nanoscale oxidation of nitroso carbon dots leads to multicolored particles (i) separated by chromatography and (ii) surface attachment of two complementary ssDNA. Reproduced with permission.[28] Copyright 2020, American Chemical Society. (c) Graphical description of the preparation, cellular uptake, and localization of the four kinds of CDs. (d) Fluorescence images of LoVo cells cocultured with the four kinds of CDs and commercial organelle probes, and 3D images of the LoVo cells incubated with the CDs and nucleus probe. Reproduced with permission.[29] Copyright 2021, American Chemical Society. (e) Schematic illustration of the live/dead cell discrimination mechanism of S-CDs. (f) Colocalization confocal images of S-CDs (20 μg mL^{-1}) and PI (30 μM) in dead *C. albicans* cells. Reproduced with permission.[30] Copyright 2022, American Chemical Society.

cell surfaces in living cells would prevent S-CDs from penetrating the inside of the cell. Thus, fluorescent signals were not emitted by living cells. S-CDs on the other hand rapidly penetrated dead cells with damaged surfaces by passive transport. As interiorized S-CDs significantly interplayed with DNA and RNA, S-CDs fluorescently illuminated dead cells, and living and dead cells could be distinguished by changes in fluorescence. More interestingly, a robust yellow fluorescent signal could be seen in the co-localized fluorescent images by PI and S-CDs, indicating that red fluorescent PI and green fluorescent S-CDs had good colocalization, which confirmed the ability of S-CDs to selectively detect dead cells (Fig. 2f). This work opened the possibility for future commercial applications of CDs. Bi *et al.* reported a microwave-assisted synthesis route for a red-emissive, RNA-targeting CD (named as M-CDs) using neutral red and levofloxacin as the precursors.[31] The M-CDs possessed a high fluorescence quantum yield of 22.83% and could bind to RNA selectively which lead to stronger red fluorescence. In addition, M-CDs could enter cells within 5 s and thus could be used for real-time tracing of the dynamic process of intracellular stress granules under oxidative stress. This research opened a new way for imaging bulk RNA dynamics and monitoring phase separation behaviors in living cells.

Apart from the achievements already made (Table 1), the field of CD fluorescence imaging is still limited by the depth of fluorescence penetration compared with those in the second near-infrared region (NIR-II). Therefore, follow-up research can be directed toward developing carbon dots with emission wavelengths located in the NIR-II region.

3.2. Magnetic resonance imaging

Magnetic resonance imaging has become more and more favored because of its great spatial resolution, nearly infinite tissue penetration depth, and it is harmless toward the organism. Besides, MRI has already been employed for clinical oncology after FDA approval in 1985.[41] Many approaches for the fabrication

Table 1 Important milestones in the field of NIR CDs

Wavelength	Biological application	Ref.
Ex_{600nm}/Em_{630nm}	Two-photon FL and PTT	67
Ex_{530nm}/Em_{650nm}	Cell imaging and PDT	32
Ex_{640nm}/Em_{705nm}	*In vivo* FL imaging	33
Ex_{680nm}	*In vivo* PA imaging	34
Ex_{700nm}/Em_{760nm}	NIR imaging-guided SDT	62
Ex_{704nm}/Em_{770nm}	*In vivo* NIR FL	35
Ex_{808nm}/Em_{805nm}	NIR FL and PTT	36
Ex_{808nm}/Em_{925m}	NIR-II FL and PTT	37
Ex_{808nm}/Em_{930nm}	*In vivo* PTT	38
Ex_{850nm}/Em_{683nm}	Two-photon cell imaging	39
Ex_{900nm}/Em_{544nm}	Multimodal imaging	65
Ex_{1064nm}	NIR-II PTT	40
Ex_{1064nm}	NIR-II PAI-guided PTT	59
Ex_{808nm}	*In vivo* FL imaging	58

of CDs with a magnetic nature have been presented. CD-based nanoparticles with extremely low cytotoxicity, good stability, and refined preparation methods as MRI contrast agents have gained popularity.[42] For example, Chen *et al.* synthesized Gd@C-dots in a size-controlled way using an approach based on mesoporous silica nanoparticles (MSN).[43] The magnetic and optical characteristics of Gd@C-dots were significantly impacted by their size. T_1-weighted MRI scans showed excellent tumor targeting (Fig. 3a). Additionally, the renal clearance process eliminated unbound nanoparticles, thus preventing long-term toxicity (Fig. 3b).

Due to their distinctive physical and chemical characteristics, gadolinium-based materials are currently frequently employed in magnetic resonance imaging. However, Gd^{3+} has the disadvantages of nephrotoxicity and its deposition in the brain, which brings potential threats and blocks their clinical applications. To solve this, Wang *et al.* designed Fe^{3+}@F,N-CDs as a T_1 contrast agent for MRI using a Fe(III) combination of fluorine and nitrogen co-doped carbon dots (F,N-CDs) (Fig. 3c).[44] MRI signals were recorded from 0 to 60 minutes after Fe^{3+}@F,N-CDs were injected into mice (Fig. 3d). At 0 minutes, the CDs accumulated in the tumor site well, but as time passed, the signal became weaker but higher than that of the pre-group, which proved the ability of Fe^{3+}@F,N-CDs to effectively aggregate in the tumor location in a remarkably short period. The significantly improved MRI effect and lower toxicity make it promising to develop into a new generation of safe MRI contrast agents.

Chemical exchange saturation transfer (CEST) MRI that combines highly specific MRS with high spatial resolution MRI has been found to provide bioimaging information of high significance clinically. Zhang *et al.* reported arginine-modified C-dots (AC-dots) as CESTMRI contrast agents.[45] As shown in Fig. 3e, the left striatum was treated with cells labeled with Lipo-AC-dots, while the right striatum was treated with cells labeled with empty liposomes as a control. 24 hours after injection, a CEST MRI was conducted (Fig. 3f). T_2-weighted (T_{2w}) images could display where the transplanted cells are located. Compared to control cells, cells tagged with Lipo-AC-dots displayed a generally stronger CEST contrast enhancement at 2 ppm. Lipo-AC-dots can be detected by CEST-MRI after *in vitro* and intracranial implantation without depositing any metal ions on the surface of carbon dots. This work guided further extension to the development of carbon dots with nuclear magnetic imaging capabilities.

Throughout the reports on the use of CDs in the field of MRI, most are based on the encapsulation of CDs or the deposition of metal ions on the CDs' surface. The direct use of CDs in MRI undoubtedly increases the biotoxicity of CDs and narrows their application in the biomedical field. Therefore, in the future, we may concentrate on improving the biosafety of the direct use of CDs for MRI and expanding the process of CD manufacture.

3.3. Multimodal imaging

Multimodality imaging integrates the advantages of independent imaging techniques. However, contrast agents have numerous hurdles to achieving multi-properties simultaneously in different imaging models.[46] Advantageously CDs are ideal multimodal imaging contrast agents owing to their effortless surface functionalization potential. For instance, Sun *et al.* developed manganese-doped CDs (Mn-CDs) for FL imaging and MRI.[47] For both FL and MRI, Chen *et al.* synthesized the Gd@GCNs by encapsulating gadolinium into CDs to afford a dual-modal contrast agent (Fig. 4a).[48] When tumor-bearing mice were injected with Gd@GCNs, strong FL and MR signals were visible from the tumor sites (Fig. 4b). Besides, Gd@GCNs could efficiently produce $^1O_2$ when exposed to light, making them a peculiar nano theranostics agent with inherently integrated FL imaging, MRI, and PDT properties.

Nickel and nitrogen co-doped carbon dots (Ni-CDs) were created by Tian *et al.* for multimodal PAI, MRI, and photothermal imaging (PTI) (Fig. 4c).[49] The photothermal signal intensity enhanced in response to the rising Ni-CDs concentration when exposed to a 1064 nm laser. Moreover, 12 hours after injecting the Ni-CDs, the photoacoustic imaging and MRI signal intensity in the tumor sites peaked (Fig. 4d). In this work, the researchers developed CDs in the second near-infrared region for multimodal imaging-guided PDT, which can be well excreted from the body after accumulating at the tumor site.

Zhang *et al.* produced PDA@N-CDs(Mn) NPs by combining the multifunctional polydopamine (PDA) which was modified by a Mn^{2+} complex with dual emissive CD-based nanoparticles for tetramodal FL imaging, PTI, and MRI (Fig. 4e).[50] PDA@N-CDs(Mn) NPs demonstrated tetramodal imaging with good contrast and spatial resolution as well as excellent tumor targeting capability.

Luo *et al.* designed a liposome carbon dot nanohybrid system (PEG-RLS/Fe) composed of Fe(II) phthalocyanine-derived Fe^{2+}-doped carbon dots (Fe@CDs) as well as amphiphilic lipopeptide assembly (DSPE-mPEG2000/RLS)@CDs).[51] This system could be successfully used for FL imaging, MRI, PTI, and PAI (Fig. 4f). The signals in FL imaging, PAI, and T_1-weighted MRI all peaked at 28 h after injecting mice with PEG-RLS/Fe@CDs, while the signal of photothermal imaging reached a peak in only 5 minutes (Fig. 4g). This work demonstrated the superiority of PEG-RLS/Fe@CDs as a FL/PA/PT/MR four-modal imaging agent, which can guide the design of CDs for multimodal imaging.

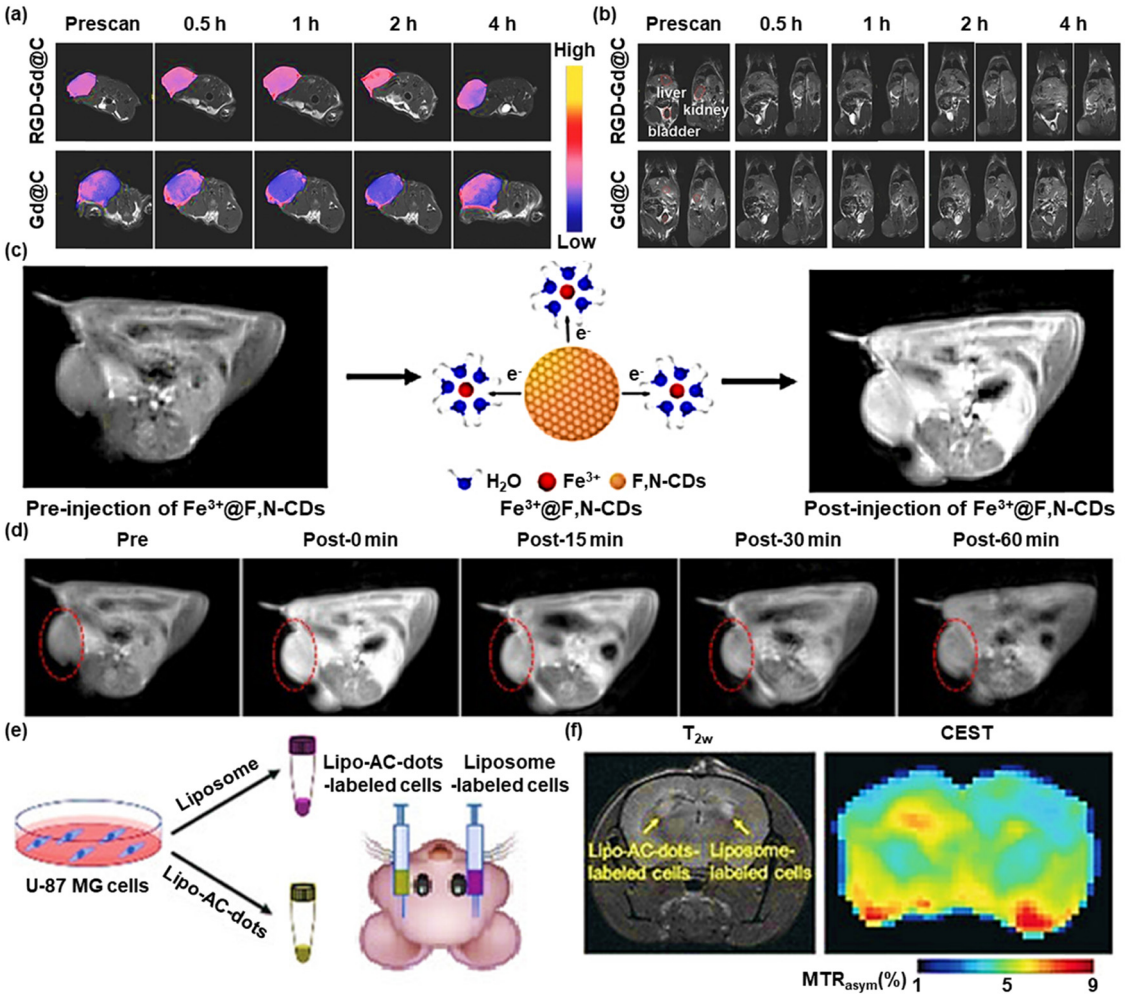

Fig. 3 (a) T_{1w} coronal MR images and (b) T_{1w} transverse MR images of the tumor-bearing mice after injecting Gd@C-dots or RGD-Gd@C-dots. Reproduced with permission.[43] Copyright 2016, Wiley-VCH. (c) Schematic illustration of MRI using Fe^{3+}@F,N-CDs as contrast agents. (d) *In vivo* MRI images of the mice after intravenous injection with Fe^{3+}@F,N-CDs at different times. The red dotted line marks the changes in MR signals. Reproduced with permission.[44] Copyright 2020, American Chemical Society. (e) Illustration of the preparation and injection of Lipo-AC-dots-labeled cells, with liposome-labeled cells as the control. (f) T_{2w} and CEST images of a mouse brain at 24 h after the implantation. Reproduced with permission.[45] Copyright 2019, Wiley-VCH.

Multimodal imaging breaks the inherent shortcomings and limitations of a single imaging mode. CDs have been widely used by researchers in the field of bioimaging due to their low synthesis cost, simple synthesis method, and ease of modification. Future research should focus on improving the comprehensive strength of CDs so that they can make more contributions to multimodal imaging.

4. CDs of cancer therapy

A series of therapy applications based on CDs are introduced to the biomedical field because of their easy functionalization, good biocompatibility, and ultrasmall size. CDs are applied mainly for their outstanding fluorescence properties, which not only have completed numerous imaging-guided tumor treatments but can also be loaded with therapeutic drugs for targeted delivery to specific sites due to their diverse modification functions. In short, CDs have unlimited potential in therapeutic areas. In this subsection, we mainly summarized the application of CDs as excellent therapeutic agents in tumor therapy.

4.1. Phototherapy

Due to the minimal invasiveness, temporal-spatial controllability, and low systemic toxicity, phototherapy, particularly PDT and PTT, has drawn interest in tumor treatment.[52] By combining chemical photosensitizers and light irradiation, phototherapy can selectively and effectively destroy lesions by transferring photon energy to molecular oxygen and creating deadly reactive oxygen species (ROS).[53] CDs are useful in phototherapy owing to satisfactory biocompatibility, ultrasmall size, and remarkable photostability. Nasrin *et al.* for the first time reported that two-photon absorption-based CDs produce increased ROS to enhance the PDT effect.[54] They synthesized CDcf derived from curcumin

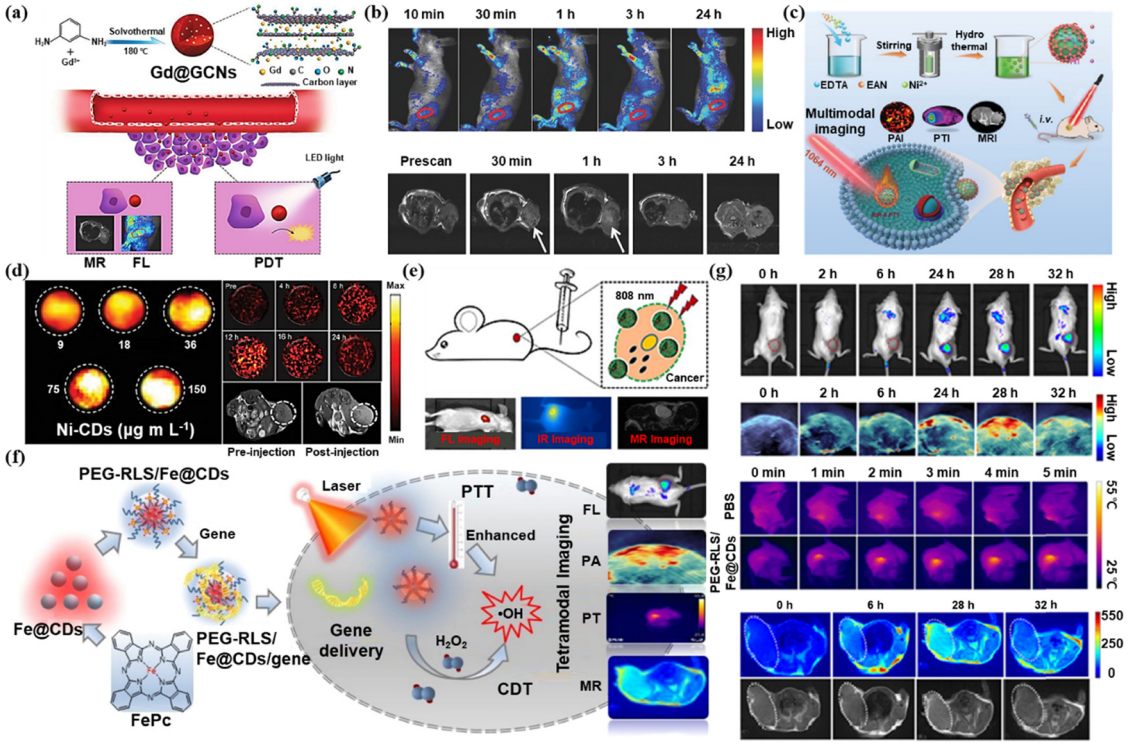

Fig. 4 (a) Schematic illustration of the Gd@GCNs for MRI and FL imaging-guide PDT. (b) *In vivo* FL and MRI images of tumor-bearing mice after intravenous injection of Gd@GCNs at different time intervals. Reproduced with permission.[48] Copyright 2018, Wiley-VCH. (c) Schematic illustration of the preparation of Ni-CDs for PTI/PAI/MRI-guided PTT of the tumor and (d) the images of PAI, PAI, and MRI. Reproduced with permission.[49] Copyright 2021, Wiley-VCH. (e) Schematic illustration of PDA@N-CDs(Mn) NPs for FL imaging, PTI, and MRI. Reproduced with permission.[50] Copyright 2019, Elsevier. (f) Schematic illustration of PEG-RLS/Fe@CDs for FL imaging, PTI, PAI, and MRI. (g) *In vivo* FL, PA, PT, and MR images after i.v. injection of PEG-RLS/Fe@CDs in mice at different time points. Reproduced with permission.[51] Copyright 2021, Elsevier.

and folic acid using a hydrothermal method with a nucleus-targeting ability (Fig. 5a). Although the significant enhancement of intracellular ROS after two-photon excitation leads to a significant increase in PDT efficiency, the achievement of real-time dynamic monitoring remained an obstacle. Yi *et al.* developed a kind of two-photon CD (TP-CD) to treat nucleolus-targeted while simultaneously monitoring dynamic changes in the nucleolus in real-time (Fig. 5b).[55] It was confirmed that particular complexation between TP-CDs and RNA had a major impact on PDT effectiveness *via* RNA damage.

PTT is a treatment modality in which the photothermal agent is irradiated at a specific wavelength, causing the temperature rise and thus killing the tumor cells.[56] Jiao *et al.* designed a kind of Gd-doped CD with AS1411 aptamers conjugating on the surface (AS1411-Gd-CDs) for FL/MR imaging-guided PTT (Fig. 5c).[57] The rise in temperature in the tumor area of the mouse models after laser treatment was monitored by thermal imaging. Fig. 5d shows how throughout laser irradiation, the temperature at the tumor sites gradually increased in all groups. It can be observed from Fig. 5e that tumor-bearing mice, after AS1411-Gd-CDs, along with laser irradiation treatment, recovered best. AS1411-Gd-CDs achieved FL/MR imaging and successfully directed efficient PTT in mice. Zhang *et al.* synthesized a kind of NIR-II fluorescent GQDs (emission at 1000 nm) dual-doped with both nitrogen and boron (N-B-GQDs).[58] N-B-GQDs could effectively absorb and convert light into heat when illuminated by a NIR laser, thus administrated a PTT effect to kill cancer cells *in vitro* and fully suppressed tumor growth. In addition, N-B-GQDs with rapid excretion capacity are very safe and suitable for *in vivo* biomedical applications.

Han *et al.* developed the NIR-II ultra-small permeable carbon dots (PCD) for fluorescence and PAI-guided PTT (Fig. 5f).[59] No obvious degradation of photothermal performance was observed after five cycles of heating and cooling, thus demonstrating the excellent photothermal stability of PCD. Additionally, the PCD group's and the NIR-II group's tumor growth was greatly slowed (Fig. 5g).

4.2. Sonodynamic therapy

Recently, sonodynamic therapy (SDT), a promising non-invasive treatment method, has been praised for its ability to produce high levels of cytotoxic ROS using low-intensity ultrasound (US) and acoustic sensitizers.[60] SDT can penetrate deeper tissues while reducing the occurrence of side effects, which shows great development potential in the field of tumor treatment. Numerous sonosensitizers, ranging from organic chemicals to inorganic nanoparticles based on metals, have been created. The special band structure of CDs allows efficient charge separation to occur at low energy excitation, which indicates their potential in SDT.

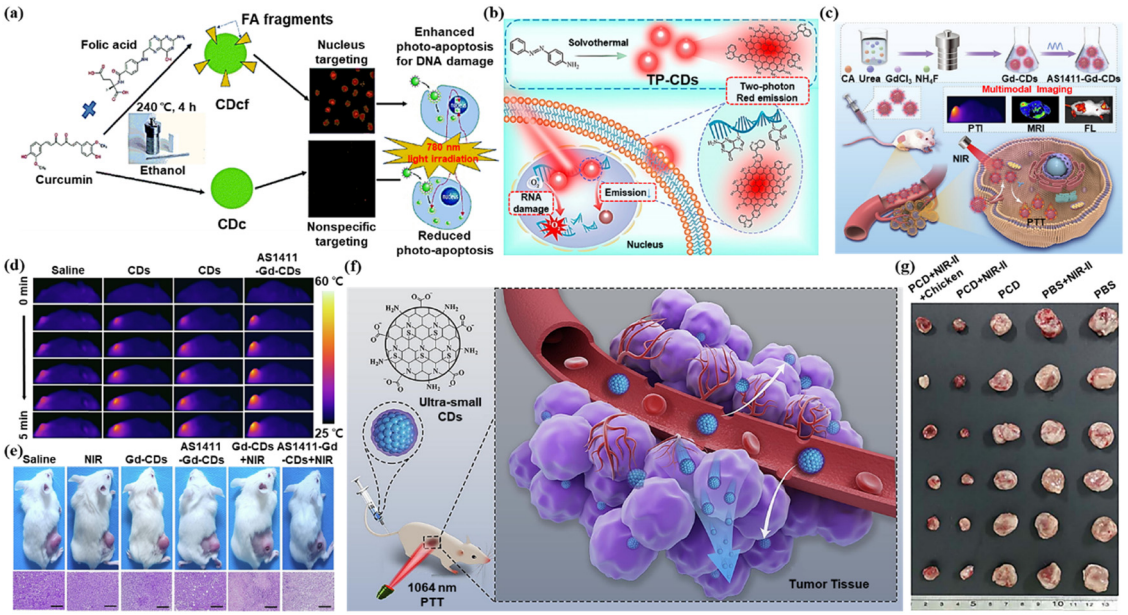

Fig. 5 (a) Illustration of CDcf synthesis for nucleus targeting and photodynamic therapy. Reproduced with permission.[54] Copyright 2020, The Royal Society of Chemistry. (b) Illustration of TP-CDs preparation and PDT in combination with real-time dynamic monitoring in the nucleolus. Reproduced with permission.[55] Copyright 2022, Elsevier. (c) Schematic illustration of the preparation of AS1411-Gd-CDs and FL/MR-guided PTT of the tumor. (d) Thermal images of the tumor-bearing nude mice upon different injections under the irradiation of a 808 nm NIR laser for 5 min (808 nm, 1 W cm^{-2}). (e) Photographs of 4T1 tumor-bearing mice and the H&E staining of the tumor at 14 days for various groups. Reproduced with permission.[57] Copyright 2022, Elsevier. (f) Schematic illustration of the application of PCD for PTT. (g) Photographs of tumors excised from the mice with different treatments. Reproduced with permission.[59] Copyright 2022, Elsevier.

Geng *et al.* constructed a Pt/N-CD@TiO_{2-x} platform by integrating p-type Pt/N-CDs with n-type TiO_{2-x} NSs for GSH detection and tumor therapy (Fig. 6a).[61] Pt/N-CD improved the ability to treat tumors under ultrasound irradiation. The tumor volume decreased throughout the treatment until it fully recovered and the survival time was prolonged to 70 days. As shown in Fig. 6b, after 16 days of different treatments, tumors in the Pt/N-CD@TiO_{2-x} treated group were eliminated. This work achieved the detection of GSH *in vivo* by Pt/N-CD and enhanced SDT functionalities by the Pt/N-CD@TiO_{2-x} platform. Based on this study, the authors prepared p–n multifunctional carbon dots (CDs) for near-infrared imaging-guided SDT (Fig. 6c).[62] As shown in Fig. 6d, the same mouse was implanted with 143B and HeLa tumors simultaneously for *in vivo* NIR imaging after being intravenously injected with p–n-CD@143B or p–n-CDs. No strong fluorescence signal at the tumor sites was observed for p–n-CDs, which may be related to their quick renal filtration. At 24 hours after injection, p–n-CD@143B was significantly retained in the 143B tumor.

Furthermore, Wang *et al.* produced sonodynamic CDs (PMQDs) utilizing vanadium carbide MXene as the carbon source.[63] As shown in Fig. 6e, PMCDs were administrated into the tail veins of mice. The tumor cells were subjected to apoptosis under the effect of ultrasound. From Fig. 6f, the US-induced PMQDs' capacity to produce ROS was visualized in MDA-MB-231 cells by DCFH-DA staining. The work also certificated that PMQDs could achieve enhanced SDT of cancer by perturbing the tumor antioxidant mechanism.

These investigations revealed that several CDs had been designed for SDT, but reports about CDs for SDT are still pretty rare and should be given more attention in the future.

4.3. Synergistic therapy

The therapeutic effects of monotherapy, such as phototherapy or sonodynamic therapy, still cannot meet all the treatment needs. The biosafety challenges of photosensitizers and sonosensitizers and the emergence of multi-drug resistance have prompted the emergence of synergistic therapy.[64] Wang *et al.* designed a multifunctional hybrid NC consisting of a magnetic Fe_3O_4 core and a mesoporous silica shell implanted with CDs and paclitaxel (PTX) and covered by another layer of silica.[65] Under NIR laser irradiation, the phototherapeutic effect of CDs combined with the chemotherapeutic effect of PTX exhibited enhanced therapeutic efficacy. Bai *et al.* prepared co-doped carbon dots with S and N atoms (S,N-CDs) as PDT/PTT agents.[66] They further developed a NIR carbon dot-metal organic framework MIL-100 (Fe)(RCDs@MIL-100) by self-assembly for chem-photothermal synergistic therapy (Fig. 7a).[67] As shown in Fig. 7b, after being treated by RCDs@MIL-100 along with light for 14 d, the tumor was completely removed. The release of Fe^{2+} from RCDs@MIL-100 in response to the tumor microenvironment (TME) was followed by a Fenton reaction to produce –OH. Chemotherapy, in combination with photothermal therapy, depleted GSH and induced oxidative stress amplification, thus leading to more –OH production as well as enhancing CDT therapy.

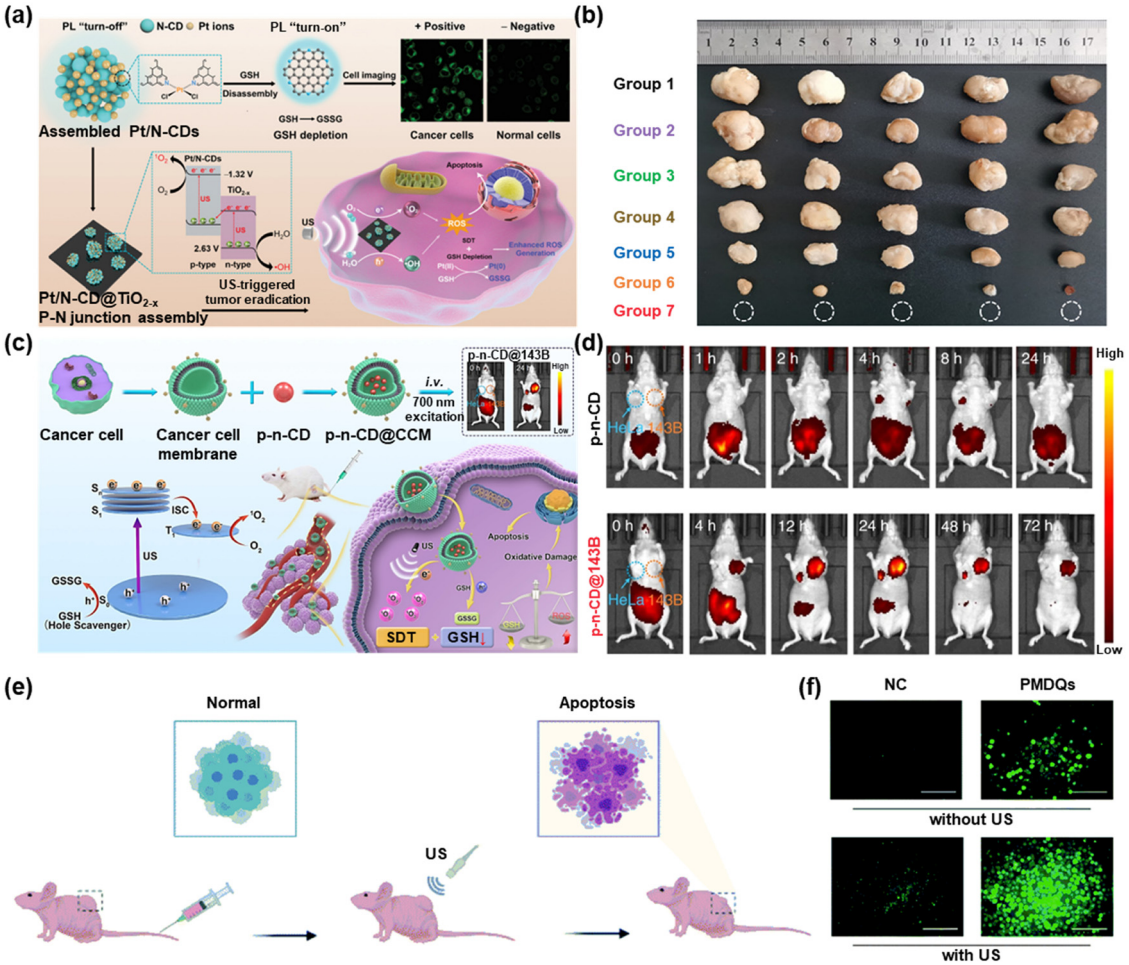

Fig. 6 (a) Schematic illustration of Pt/N-CD@TiO_{2-x} for SDT. (b) Solid tumor pictures of different treatment groups. Reproduced with permission.[61] Copyright 2022, Wiley-VCH. (c) Schematic illustration of SDT by p–n-CD@CCM. (d) *In vivo* NIR imaging of mice with p–n-CDs and p–n-CDs@CCM. Reproduced with permission.[62] Copyright 2022, Springer Nature. (e) Schematic illustration of the application of PMQDs for enhanced SDT of cancer in tumor-bearing mice. (f) Fluorescence images of DCFH-DA stained MDA-MB-231 cells treated with PMQDs under US irradiation. Reproduced with permission.[63] Copyright 2022, The Royal Society of Chemistry.

Sun *et al.* launched Ce6-RCDs by attaching chlorin e6 (Ce6) to amino-rich red emissive carbon dots (RCDs) for multimodal FL/PA/PT imaging-guided PTT/PDT (Fig. 7c).[68] Under low-power laser illumination, tumor-bearing mice receiving PDT or PTT monotherapy showed significant recurrence after 13 days, while groups treated with PDT-PTT displayed no signs of tumor recurrence (Fig. 7d). This work provided strong evidence for the advantage of synergistic PDT/PTT over single-mode PDT or PTT. Huang *et al.* designed a targeting peptide (IP)-modified mesoporous silica-coated graphene nanosheet (GSPI) for chemo-photothermal targeted therapy of glioma.[69] Then a doxorubicin (DOX)-loaded GSPI-based system (GSPID) was constructed to realize heat-stimulative, pH-responsive, and continuous release properties. This IP modification design greatly enhanced the accumulation of GSPID in the glioma cells, which are beneficial for the elimination of cancer cells. Wang *et al.* synthesized GQDs@DOX/PB by encapsulating GQDs with doxorubicin (DOX) into the cores of poly lactic-*co*-glycolic acid (PLGA) nanoparticles which were coated with bovine serum albumin (BSA).[70] The GQDs@DOX/PB NPs showed good photothermal properties and stability and induced the thermal ablation of tumor cells upon illumination with an NIR laser during the chemophotothermal synergetic therapy.

Synergistic therapy is now a very promising choice in tumor treatment, which can overcome the shortcomings of mono-therapy and enhance the therapeutic effect. In the future, the advantages of sonodynamic therapy can be introduced to inject new blood into synergistic therapy.

5. CDs for antibacterial application

Bacterial infection is a serious problem in the biomedical field and is also an important factor hindering wound healing. In recent years, CDs have become a rising star in antibacterial applications.[71]

Yu *et al.* developed folic acid-derived carbon dots (FA-CDs) using a one-step pyrolysis technique. In the simulated infection

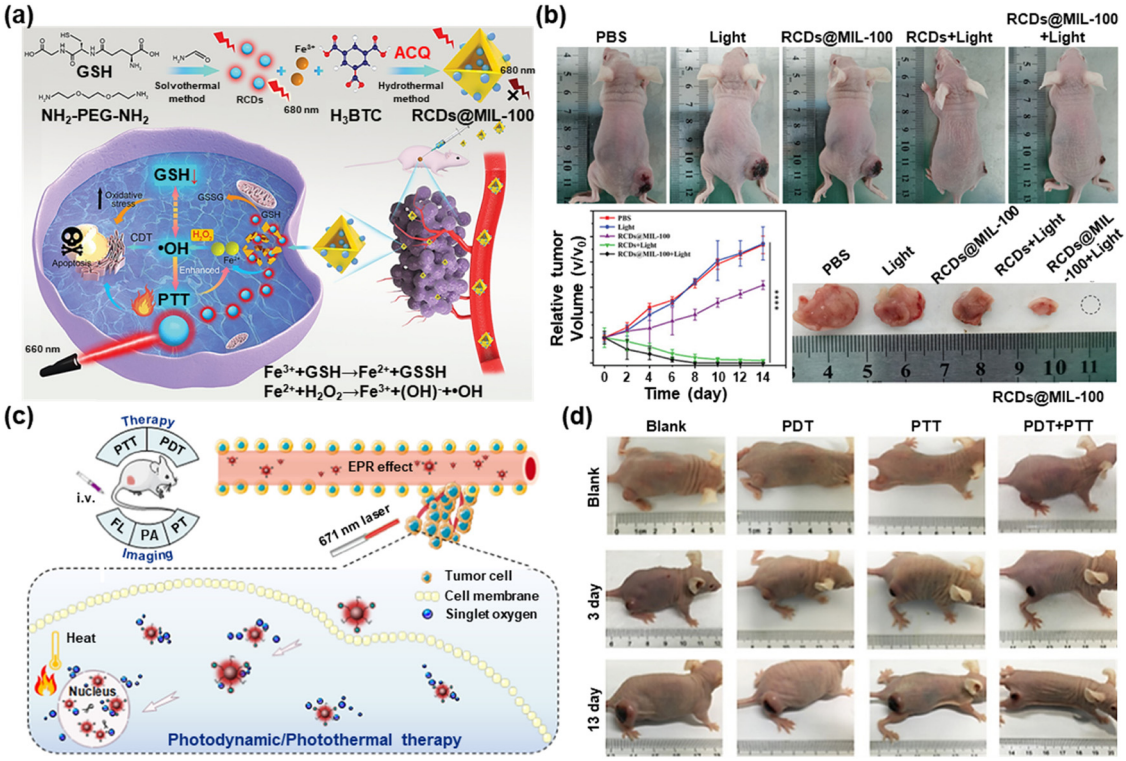

Fig. 7 (a) Schematic demonstration of the RCDs@MIL-100 for chem-photothermal combined therapy. (b) Photographs and tumor volume records of mice in different groups after various treatments for 14 days and photographs of dissected tumors after corresponding treatments for 14 days. Reproduced with permission.[67] Copyright 2022, Wiley-VCH. (c) Schematic representation of the Ce6-RCDs for the synergistic PTT/PDT process. (d) Digital photographs of tumor-bearing mice after different treatments for 13 days. Reproduced with permission.[68] Copyright 2019, American Chemical Society.

site's acidic environment, FA-CDs showed responsive antibacterial properties and were able to successfully clear the built-up biofilm (Fig. 8a).[72] FA-CDs were employed as a sensitive antibacterial nanoplatform with pH responsiveness. As shown in Fig. 8b, the viable colonies of *Staphylococcus aureus* co-incubated with FA-CDs decreased significantly with the prolongation of incubation time. The low toxicity of FA-CDs to normal cells and bacteria in a neutral environment reduced the bacterial resistance and the side effects of antimicrobial therapy.

A unique xerogel AgNPs/N-CD@ZnO PTLA (P2) was created by Huang *et al.* using thioether as the main chain and inserted by Ag nanoparticles (NPs) and ZnO NPs embellished with N-doped carbon dots (N-CD@ZnO), which was effective against *Escherichia coli* and *Staphylococcus aureus*.[73] When the xerogel was irradiated with an 808 nm laser, N-CD@ZnO invaded the interior of bacteria through the damaged membrane after generating a large amount of ROS and then synergized with Ag^+ to effectively destroy the bacteria (Fig. 8c). Additionally, as demonstrated in Fig. 8d, the control and 3M dressing groups manifested an evident bacterial infection after 2 days of trauma treatment, while the *E. coli* (P2) group had reduced efficacy. The P2 group had nearly fully recovered after 10 days of therapy, whereas the other groups had only partially recovered, showing that the effect of wound healing was better when supplemented by 808 nm irradiation for rapid sterilization.

Liu *et al.* designed and produced copper-doped carbon dots (Cu-CDs), which achieved biofilm eradication, alternative bactericidal, wound healing, and whitening capabilities for the treatment of oral diseases (Fig. 8e).[74] Modified Cu-CDs with orally adapted POD- and CAT-like activities gave rise to the production of O_2 and ROS. Meanwhile, several endogenous and exogenous dental stains were whitened without damage based on ROS generated by the Cu-CD/H_2O_2 system (Fig. 8f). According to the photographs shown in Fig. 8g, the degree of discoloration in the first hour in the Cu-CD + H_2O_2 group was much stronger than that in the H_2O_2 and CD + H_2O_2 groups. The teeth's interior color continued to lighten under the impact of the Cu-CD + H_2O_2 bleaching solution as the bleaching duration increased, and a good tooth color could be obtained at 5 h. A more practical and affordable daily plan for dental health care was established by this effort.

There is no doubt that CDs have been widely used in the antibacterial field, which have excellent bactericidal properties and the ability to accelerate wound healing. However, there are few reports on the direct application of CDs in sterilization. In addition, photothermal antibacterial and sonodynamic antibacterial methods are not yet widely used in the field of CDs antibacterial. These are all the questions to be explored in the future.

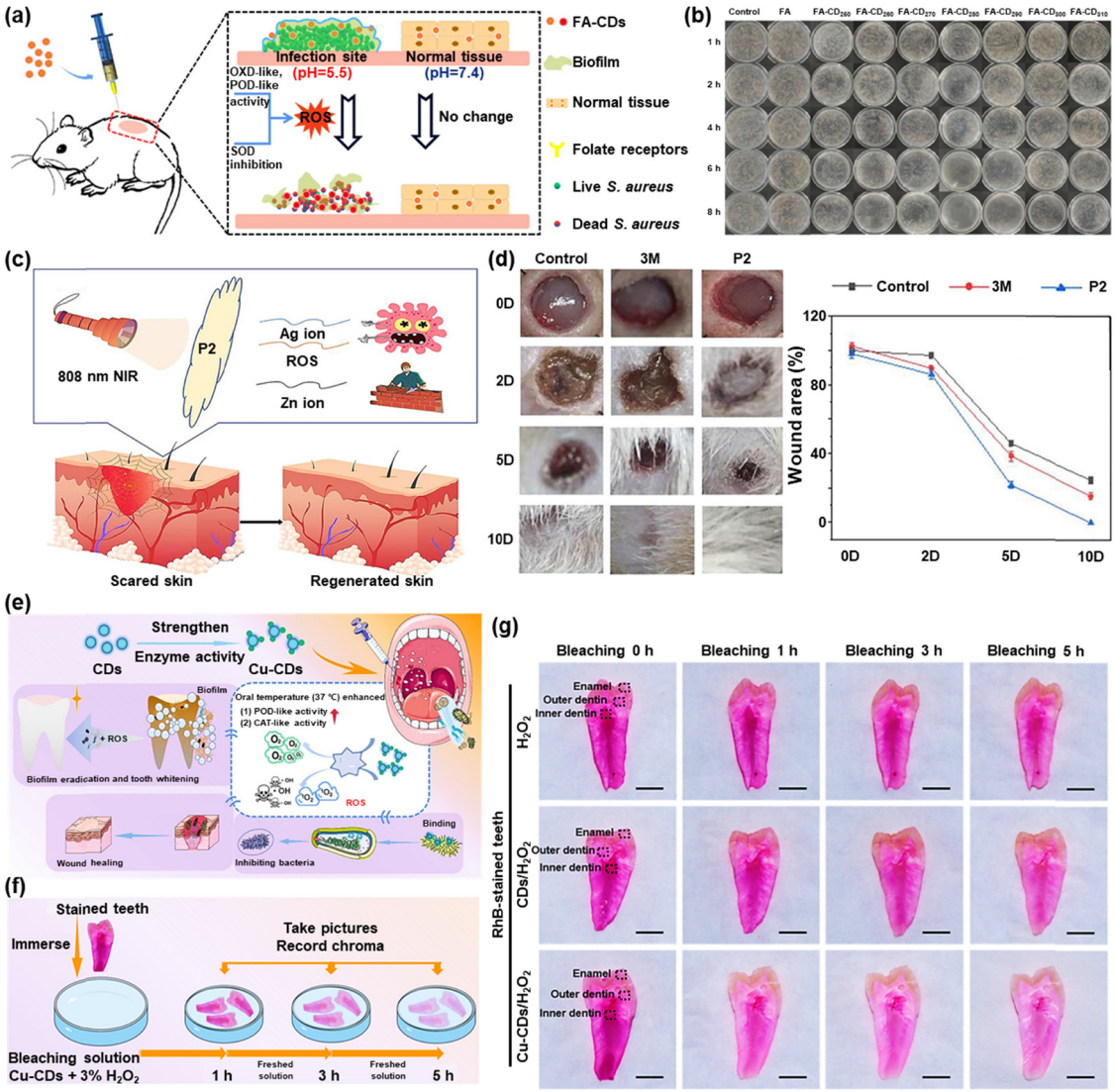

Fig. 8 (a) Schematic diagram of *S. aureus* being killed and biofilm being removed by FA-CDs. (b) Agar plate photographs of *S. aureus* colonies grown with FA-CDs at different times in pH 5.5. Reproduced with permission.[72] Copyright 2022, Elsevier. (c) Schematic diagram of wound healing by P2. (d) Photographs of wound sizes at different times after different treatments. Reproduced with permission.[73] Copyright 2022, Elsevier. (e) Schematic diagram of the process of Cu-CDs for multifunctional prevention and treatment of oral diseases. (f) Experimental method for tooth internal whitening. (g) Photographs of the interior of RhB-stained teeth at different times. Reproduced with permission.[74] Copyright 2022, American Chemical Society.

6. Mechanism for improving the quantum yield of CDs

CDs with an especially high fluorescence quantum yield (QY), could maximize their desired applications in chemo/biosensors, bioimaging, drug delivery, cancer therapy, optoelectronic devices and white light-emitting diodes, *etc.* However, efficient methods for the synthesis of CDs with a high QY still remain as a challenge.[75] Most reported CDs are limited by a relatively low QY. Therefore, extensive efforts have been devoted in the development of high fluorescent CDs. To date, chemical doping with heteroatoms is the major renowned pathway to tune the intrinsic properties of CDs. Heteroatoms such as P, B, N and S can be inherited from precursors during synthesis, and have been studied to be doped in CDs.[76] For instance, Wei *et al.* applied the Maillard reaction between glucose and amino acids to systematically synthesize a series of N-doped C-dots with a high QY (~69.1%) and PL tunable by N-doping level (shorter emission wavelength with higher N-doping by using basic amino acids).[77] It has been shown that N-doping (mainly pyrrolic, possibly pyridinic, but not graphitic doping configuration) on GQDs increases the QY and causes a blue shift in emission due to the electron-withdrawing ability of nitrogen atoms.[76]

Other elements (*e.g.*, Si, P, S and B) have also been doped in C-dots and GQDs to change the PL characteristics or gain catalytic properties. Yu *et al.* reported S and N co-doped C-dots, which exhibit very high FLQY (73%) and excitation independent emission, resulting from the synergy effect of the doped nitrogen and sulfur atoms. They further suggested

this mechanism could be attributed to the doping of nitrogen and can introduce the CDs to a new kind of surface state, whose density can be increased dramatically by the co-doped sulfur atoms, which offers great scientific insights to the FL enhancement mechanism of CDs.[78] The doping of silicon (Si), which belongs to the same group as C, group IV, but strongly prefers sp^3-like bonding, is considered to influence the electronic and structural properties of carbon-based material in a different way from that of N doping. In view of the remarkable quantum-confinement and edge effects of carbon quantum dots, doping CQDs with Si atoms could alter their electronic characteristics and offer more active sites, thus producing new and unexpected properties and serving as novel nanodevices such as chemical sensors and toxic gas scrubbers. For example, Feng *et al.* proposed a simple and efficient route to prepare silicon-doped carbon quantum dots (SiCQDs) with strong photoluminescence through a solvent-thermal reaction.[79] The fluorescence is substantially enhanced through the doping of silicon relative to that of CQDs without silicon atoms, and the quantum yield of SiCQDs is up to 19.2%. Although the phosphorus atom is larger than the carbon atom, it has been shown that phosphorous can form substitutional defects in diamond sp^3 thin films, behaving as an n-type donor and thereby modifying the electronic and optical properties. In view of the remarkable quantum-confinement and edge effects of carbon quantum dots, doping CQDs with P atoms could alter their electronic characteristics and offer more active sites, thus producing new and unexpected properties. P-doped carbon quantum dots (PCQDs) were synthesized by Feng *et al.* using phosphorous tribromide and hydroquinone as precursors. The as-prepared PCQDs present strong visible fluorescence with a quantum yield up to 25%. The toxicity and bioimaging experiments showed that PCQDs have low cell toxicity and excellent biolabeling ability.[80]

7. Mass production of CDs

The cost to create CDs becomes the barrier for making CDs a reality and for commercial use. Thus methods for mass production have been of great interest. Many things can be

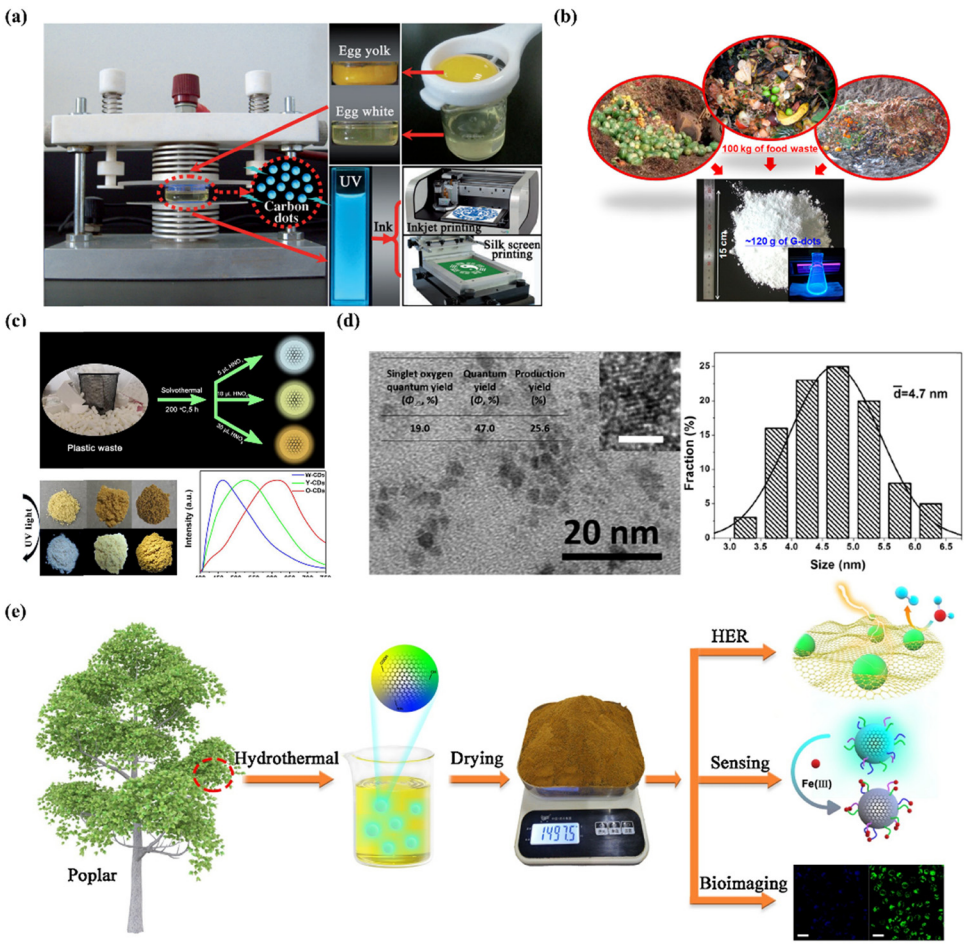

Fig. 9 (a) Schematic description of plasma-induced fabrication of egg-derived CDs.[82] Copyright 2012, Wiley-VCH. (b) Schematic diagram of the transition from food waste to useful carbon-based nanomaterials.[83] Copyright 2014, American Chemical Society. (c) Schematic diagram of solid-state fluorescent CDs prepared from plastic waste.[84] Copyright 2019, Elsevier. (d) TEM image of the CDs (scale bar, 2 nm) and the size distribution of CDs.[85] Copyright 2017, Elsevier. (e) Schematic description of the synthesis of CQDs.[86] Copyright 2019, Elsevier.

used as raw materials to produce CDs, such as food wastes, ethanol, egg, plastic waste, coal, and poplar leaves.[81] Chen *et al.* developed a fast method for obtaining fluorescently stable CDs by using edible, low-cost, and natural chicken eggs as the precursor.[82] Egg white or yolk separated from an egg in a glass dish was placed between two quartz slides of the plasma generator (Fig. 9a). Then the egg samples were irradiated with plasma beams generated from the upper electrode (voltage = 50 V, current = 2.4 A) for 3 min to yield dark black products (conversion yields, 5.96%). Lee *et al.* created an approach to realize large-scale synthesis of water-soluble CDs by reusing food waste (Fig. 9b).[83] The food waste is first subjected to ultrasound irradiation to dehydrate, polymerize and carbonize, leading to a short single burst of nucleation. Then, the nuclei grow by the diffusion of solutes to the surfaces of the carbon nanoparticle. The resulting nanocarbon is highly functionalized with good water solubility. In the end, about 120 g of CDs can be synthesized per 100 kg of food waste (conversion yields, 0.12%). Lu *et al.* prepared solid-state fluorescent CDs with photoluminescence tunable from white to orange from plastic waste through a one-step solvothermal method (conversion yields, 60–85%) (Fig. 9c).[84] The conversion of plastic waste has a good application prospect in the mass production of CDs, and also provides a feasible method for the recycling of plastic waste. Qiu *et al.* employed a simple and easy one-pot solvothermal method to synthesize fluorescent nitrogen-doped CDs in the presence of DMF using Taixi anthracite as the raw material (conversion yields, 25.6%).[85] This approach is green and sustainable by obtaining the product through rotary evaporation and recycling the solvent (Fig. 9d). The resulting CDs exhibited a strong photoluminescence (quantum yield, 47.0%) and a singlet oxygen generation behavior (quantum yield, 19.0%). Yang *et al.* reported an easy, environmentally friendly, kilogram-scale synthesis of fluorescent CQDs using poplar leaves in a one-step hydrothermal route (conversion yields, 29.95%) (Fig. 9e).[86] The throughput of the CQDs can reach up to 1.4975 kg in 1 pot and the CQDs possessed a high photoluminescent quantum yield (10.64%), good stability, abundant functional groups, low cytotoxicity as well as constant photoluminescence within the biological pH range.

8. Conclusion and outlook

Researchers in the biomedical field are becoming increasingly interested in CDs due to their various benefits, which include extraordinary water solubility, good photostability, high biocompatibility, and simple surface functional group modification. In this essay, we go through current advancements in the application of CDs in disease-associated biomarker and biomolecule detection, bioimaging, and imaging-guided therapy. CDs are, without a doubt, thriving and promising materials in the biomedical industry. However, there are still a number of barriers preventing their widespread application and clinical translation.

First, the absorption/emission wavelengths of the present CDs are primarily centered within the visible and NIR-I ranges, which impedes their use in deep-tissue diagnostics and therapy.[87] Shifting the emissive wavelength of CDs to the NIR-II areas will improve their *in vivo* fluorescence imaging contrast and resolution without question. Moreover, the bathochromic shift of CD absorption might increase not only the photothermal therapy's efficacy but also the therapy's performance in deep-site lesions. To date, NIR-II emissive CDs have been severely scarce and must be created.

Since its introduction, sonodynamic therapy has been recognized as an enticing current treatment option for eradicating cancer in a very effective manner. In the realm of SDT, CD applications are still in their infancy. CDs possess unique advantages compared to other forms of sonosensitizers. For instance, imaging modality and SDT might be readily incorporated into the CD platform in order to execute imaging-guided SDT. Moreover, similar to PDT, the efficacy of SDT is similarly dependent on O_2, and this issue has recently been solved by the invention of CD photocatalysts or p–n junction CDs.

Although CDs have found success in imaging and therapy, their optimization for enhancing *in vivo* imaging and therapeutic efficacy remains to be further studied. The incorporation of biorthogonal functional groups or self-assembled units (*e.g.*, peptide) into CDs could equip them with collective behavior under particular conditions, including the overexpression of small molecules or enzymes. On the basis of these methodologies, the imaging signals and therapeutic effects of CDs might be significantly boosted to realize a precise and secure *in vitro* and *in vivo* theranostic plan.

Immuno-oncology, a method of treating cancer by stimulating the immune system, is another promising area of research. CD-mediated immunotherapy for cancer has been described infrequently until now. It is of utmost importance to investigate whether CDs interact with immunotherapeutic targets and the underlying mechanism for this interaction.

The current epidemic COVID-19 has highlighted the urgent need for the development of effective antiviral therapies. Antiviral effects can be conferred by carbon-based nanomaterials of the same size as viruses, such as compact discs. However, research on the antiviral activity of CDs remains in its infancy, and more effort should be done in the future to investigate their processes in the antiviral field.

Conflicts of interest

There are no conflicts to declare.

Acknowledgements

This work is supported by the National Natural Science Foundation (22022404, 22074050, 82172055, 81870939, and 31900051), fundamental research funds for the Central Universities (CCNU22QN007), Guangxi Key Laboratory of Automatic Detecting Technology and Instruments (YQ21206) and

the National Research Foundation of Korea (NRF) (CRI Project No. 2018R1A3B1052702, J. S. K.).

References

1 X. Y. Xu, Y. L. Gu, H. J. Ploehn, L. Gearheart, K. Raker and W. A. Scrivens, *J. Am. Chem. Soc.*, 2004, **126**, 12736.
2 X. T. Zheng, A. Ananthanarayanan, K. Q. Luo and P. Chen, *Small*, 2015, **11**, 1620.
3 (*a*) D. Li, E. V. Ushakova, A. L. Rogach and S. Qu, *Small*, 2021, **17**, 2102325; (*b*) K. Hola, A. B. Bourlinos, O. Kozak, K. Berka, K. M. Siskova, M. Havrdova, J. Tucek, K. Safarova, M. Otyepka, E. P. Giannelis and R. Zboril, *Carbon*, 2014, **70**, 279.
4 (*a*) M. Pirsaheb, S. Mohammadi and A. Salimi, *TrAC, Trends Anal. Chem.*, 2019, **115**, 83; (*b*) S. Y. Tao, T. L. Feng, C. Y. Zheng, S. J. Zhu and B. Yang, *J. Phys. Chem. Lett.*, 2019, **10**, 5182.
5 (*a*) C. L. Xia, S. J. Zhu, T. L. Feng, X. Yang and B. Yang, *Adv. Sci.*, 2019, **6**, 1901316; (*b*) J. Di, J. X. Xia, Y. P. Ge, H. P. Li, H. Y. Ji, H. Xu, Q. Zhang, H. M. Li and M. N. Li, *Appl. Catal., B*, 2015, **51**, 16; (*c*) A. K. Samantara, S. S. Chandra, A. Ghosh and B. K. Jena, *J. Mater. Chem. A*, 2015, **3**, 16961.
6 (*a*) M. Bacon, S. J. Bradley and T. Nann, *Part. Part. Syst. Charact.*, 2014, **31**, 415; (*b*) E. Haque, J. Kim, V. Malgras, K. R. Reddy, A. C. Ward, J. You, Y. Bando, M. S. A. Hossain and Y. Yamauchi, *Small Methods*, 2018, **2**, 1800050.
7 (*a*) A. Kaczmarek, J. Hoffman, J. Morgiel, T. Moscicki, L. Stobinski, Z. Szymanski and A. Malolepszy, *Materials*, 2021, **14**, 729; (*b*) H. W. Yu, X. Y. Li, X. Y. Zeng and Y. F. Lu, *Chem. Commun.*, 2016, **52**, 819.
8 (*a*) C. B. Ke, T. L. Lu and J. L. Chen, *Nanomaterials*, 2018, **8**, 372; (*b*) J. S. Wei, C. Ding, P. Zhang, H. Ding, X. Q. Niu, Y. Y. Ma, C. Li, Y. G. Wang and H. M. Xiong, *Adv. Mater.*, 2019, **31**, 1806197.
9 (*a*) Z. H. Geng, X. Wang, X. C. Guo, Z. Zhang, Y. J. Chen and Y. F. Wang, *J. Mater. Chem. B*, 2016, **4**, 3331; (*b*) M. L. Liu, Y. H. Xu, F. S. Niu, J. Justin Gooding and J. Q. Liu, *Analyst*, 2016, **141**, 2657.
10 (*a*) Y. Q. Wang, X. C. Li, S. J. Zhao, B. H. Wang, X. Z. Song, J. F. Xiao and M. H. Lan, *Coord. Chem. Rev.*, 2022, **470**, 214703; (*b*) X. T. Tian and X. B. Yin, *Small*, 2019, **15**, 1901803.
11 (*a*) P. Innocenzi and L. Stagi, *Chem. Sci.*, 2020, **11**, 6606; (*b*) M. Algarra, M. Perez-Martin, M. Cifuentes-Rueda, J. Jimenez-Jimenez, J. C. Esteves da Silva, T. J. Bandosz, E. Rodriguez-Castellon, J. T. Lopez Navarrete and J. Casado, *Nanoscale*, 2014, **6**, 9071.
12 (*a*) J. Tan, Q. J. Li, S. Meng, Y. Li, J. C. Yang, Y. X. Ye, Z. K. Tang, S. N. Qu and X. D. Ren, *Adv. Mater.*, 2021, **33**, 2006781; (*b*) T. V. de Medeiros, J. Manioudakis, F. Noun, J. R. Macairan, F. Victoria and R. Naccache, *J. Mater. Chem. C*, 2019, **7**, 7175.
13 (*a*) B. Y. Wang, H. J. Cai, G. I. N. Waterhouse, X. L. Qu, B. Yang and S. Y. Lu, *Small Science*, 2022, **2**, 2200012; (*b*) X. Zhang, X. W. Wei, J. J. Qi, J. Shen, J. W. Xu, G. Y. Gong, Y. Wei, J. Yang, Q. Y. Zhu, T. T. Bai, Z. R. Guo, X. J. Qu and Y. F. Zhu, *Anal. Chem.*, 2022, **94**, 4787.
14 (*a*) S. Hamd-Ghadareh, A. Salimi, F. Fathi and S. Bahrami, *Biosens. Bioelectron.*, 2017, **96**, 308; (*b*) M. S. Wu, Z. R. Zhou, X. Y. Wang, B. B. Chen, M. E. Hafez, J. F. Shi, D. W. Li and R. C. Qian, *Anal. Chem.*, 2022, **94**, 2882; (*c*) J. S. Lin, Y. W. Tsai, K. Dehvari, C. C. Huang and J. Y. Chang, *Nanoscale*, 2019, **11**, 20917; (*d*) Q. Xu, J. J. Gao, S. Y. Wang, Y. Wang, D. Liu and J. C. Wang, *J. Mater. Chem. B*, 2021, **9**, 5765.
15 (*a*) W. J. Liu, H. Gu, W. K. Liu, C. Y. Lv, J. J. Du, J. L. Fan and X. J. Peng, *Chem. Eng. J.*, 2022, **450**, 137384; (*b*) J. H. Liu, D. Y. Li, J. H. He, D. Yuan, R. S. Li, S. J. Zhen, Y. F. Li and C. Z. Huang, *ACS Appl. Mater. Interfaces*, 2020, **12**, 4815; (*c*) S. Chen, T. T. Sun, M. Zheng and Z. G. Xie, *Adv. Funct. Mater.*, 2020, **30**, 2004680; (*d*) Y. C. Niu, J. P. Li, J. J. Gao, X. C. Ouyang, L. L. Cai and Q. Xu, *Nano Res.*, 2021, **14**, 3820.
16 P. L. Gao, S. Chen, S. Liu, H. X. Liu, Z. G. Xie and M. Zheng, *ACS Appl. Mater. Interfaces*, 2021, **13**, 56456.
17 (*a*) Y. J. Chung, J. Kim and C. B. Park, *ACS Nano*, 2020, **14**, 6470; (*b*) J. J. Du, N. Xu, J. L. Fan, W. Sun and X. J. Peng, *Small*, 2019, **15**, 1805087; (*c*) W. Su, H. Wu, H. M. Xu, Y. Zhang, Y. C. Li and L. Z. Fan, *Mater. Chem. Front.*, 2020, **4**, 821; (*d*) L. Đorđević, F. Arcudi and M. Prato, *Nat. Nanotechnol.*, 2022, **17**, 112.
18 X. Geng, Y. Q. Sun, Y. F. Guo, Y. M. Zhao, K. Zhang, L. H. Xiao, L. B. Qu and Z. H. Li, *Anal. Chem.*, 2020, **92**, 7940.
19 C. H. Sun, L. L. Pan, L. Zhang, J. J. Huang, D. D. Yao, C. Z. Wang, Y. Zhang, N. Jiang, L. N. Chen and C. S. Yuan, *Analyst*, 2019, **144**, 6760.
20 Y. Z. Guo, J. L. Liu, Y. F. Chen, Y. Q. Chai, Z. H. Li and R. Yuan, *Anal. Chem.*, 2022, **94**, 7601.
21 M. J. Zou, Y. Gong, X. X. Sun and C. F. Ding, *Sens. Actuators, B*, 2022, **369**, 132330.
22 W. Q. Yang, J. C. Ni, F. Luo, W. Weng, Q. H. Wei, Z. Y. Lin and G. N. Chen, *Anal. Chem.*, 2017, **89**, 8384.
23 G. X. Yin, Y. B. Gan, H. M. Jiang, T. Yu, M. L. Liu, Y. Y. Zhang, H. T. Li, P. Yin and S. Z. Yao, *Anal. Chem.*, 2021, **93**, 9878.
24 R. N. Jia, K. F. Jin, J. M. Zhang, X. J. Zheng, S. Wang and J. Zhang, *Sens. Actuators, B*, 2020, **321**, 128506.
25 (*a*) N. N. Yu, T. H. Huang, T. F. Duan, Y. Bao, R. C. Gao, X. Z. Wang, K. Xu and C. P. Han, *Chem. Eng. J.*, 2022, **440**, 135801; (*b*) D.-K. Ji, G. Reina, H. Liang, D. Zhang, S. Guo, B. Ballesteros, C. Ménard-Moyon, J. Li and A. Bianco, *ACS Appl. Nano Mater.*, 2021, **4**, 1467; (*c*) Y. L. Liu, X. Zhi, W. X. Hou, F. F. Xia, J. P. Zhang, L. X. Li, Y. P. Hong, H. Yan, C. Peng, J. M. de la Fuentea, J. Song and D. X. Cui, *Nanoscale*, 2018, **10**, 19052.
26 P. Bag, R. K. Maurya, A. Dadwal, M. Sarkar, P. A. Chawla, R. K. Narang and B. Kumar, *ChemistrySelect*, 2021, **6**, 2774.
27 X. Zhang, X. F. Liao, Y. J. Hou, B. Y. Jia, L. Z. Fu, M. X. Jia, L. D. Zhou, J. H. Lu and W. J. Kong, *J. Hazard. Mater.*, 2022, **422**, 126881.

28 I. Srivastava, S. K. Misra, S. Bangru, K. A. Boateng, J. Soares, A. S. Schwartz-Duval, A. Kalsotra and D. Pan, *ACS Appl. Mater. Interfaces*, 2020, **12**, 16137.
29 E. Shuang, C. He, J. H. Wang, Q. X. Mao and X. W. Chen, *ACS Nano*, 2021, **15**, 14465.
30 X. W. Yu, X. Y. Liu, Y. W. Jiang, Y. H. Li, G. Gao, Y. X. Zhu, F. M. Lin and F. G. Wu, *Anal. Chem.*, 2022, **94**, 4243.
31 L. Jiang, H. Cai, W. W. Zhou, Z. J. Li, L. Zhang and H. Bi, *Adv. Mater.*, 2023, DOI: **10.1002/adma.202210776**.
32 Y. Q. Sun, H. Y. Qin, X. Geng, R. Yang, L. B. Qu, A. N. Kani and Z. H. Li, *ACS Appl. Mater. Interfaces*, 2020, **12**, 31738.
33 J. J. Liu, Y. J. Geng, D. W. Li, H. Yao, Z. P. Huo, Y. F. Li, K. Zhang, S. J. Zhu, H. T. Wei, W. Q. Xu, J. L. Jiang and B. Yang, *Adv. Mater.*, 2020, **32**, 1906641.
34 C. Lee, W. Kwon, S. Beack, D. Lee, Y. Park, H. Kim, S. K. Hahn, S. W. Rhee and C. Kim, *Theranostics*, 2016, **6**, 2196.
35 H. Q. Tao, K. Yang, Z. Ma, J. M. Wan, Y. J. Zhang, Z. H. Kang and Z. Liu, *Small*, 2012, **8**, 281.
36 M. Zheng, Y. Li, S. Liu, W. Q. Wang, Z. G. Xie and X. B. Jing, *ACS Appl. Mater. Interfaces*, 2016, **8**, 23533.
37 Y. B. Li, G. X. Bai, S. J. Zeng and J. H. Hao, *ACS Appl. Mater. Interfaces*, 2019, **11**, 4737.
38 S. J. Zhao, L. Yan, M. Y. Cao, L. Huang, K. Yang, S. L. Wu, M. H. Lan, G. L. Niu and W. J. Zhang, *ACS Appl. Mater. Interfaces*, 2021, **13**, 53610.
39 L. L. Pan, S. Sun, L. Zhang, K. Jiang and H. W. Lin, *Nanoscale*, 2016, **8**, 17350.
40 B. J. Geng, W. W. Shen, F. L. Fang, H. Qin, P. Li, X. L. Wang, X. K. Li, D. Y. Pan and L. X. Shen, *Carbon*, 2020, **162**, 220.
41 (*a*) K. Akazawa, F. Sugihara, T. Nakamura, H. Matsushita, H. Mukai, R. Akimoto, M. Minoshima, S. Mizukami and K. Kikuchi, *Angew. Chem., Int. Ed.*, 2018, **57**, 16742; (*b*) G. Angelovski and E. Toth, *Chem. Soc. Rev.*, 2017, **46**, 324; (*c*) S. E. Kirberger, S. D. Maltseva, J. C. Manulik, S. A. Einstein, B. P. Weegman, M. Garwood and W. C. K. Pomerantz, *Angew. Chem., Int. Ed.*, 2017, **56**, 6440.
42 (*a*) W. H. Zeng, L. Y. Wu, Y. Ishigaki, T. Harimoto, Y. X. Hu, Y. D. Sun, Y. Q. Wang, T. Suzuki, H. Y. Chen and D. J. Ye, *Angew. Chem., Int. Ed.*, 2022, **61**, e202111759; (*b*) N. Nimi, A. Saraswathy, S. S. Nazeer, N. Francis, S. J. Shenoy and R. S. Jayasree, *Biomaterials*, 2018, **171**, 46.
43 H. M. Chen, G. D. Wang, X. L. Sun, T. Todd, F. Zhang, J. Xie and B. Z. Shen, *Adv. Funct. Mater.*, 2016, **26**, 3973.
44 J. M. Wang, X. L. Hu, H. Z. Ding, X. Huang, M. S. Xu, Z. Z. Li, D. Wang, X. Yan, Y. Lu, Y. J. Xu, Y. Chen, P. C. Morais, Y. P. Tian, R. Q. Zhang and H. Bi, *ACS Appl. Mater. Interfaces*, 2019, **11**, 18203.
45 J. Zhang, Y. Yuan, M. L. Gao, Z. Han, C. Y. Chu, Y. G. Li, P. C. M. van Zijl, M. Y. Ying, J. W. M. Bulte and G. S. Liu, *Angew. Chem., Int. Ed.*, 2019, **58**, 9871.
46 (*a*) D. S. Karaman, M. P. Sarparanta, J. M. Rosenholm and A. J. Airaksinen, *Adv. Mater.*, 2018, **30**, 1703651; (*b*) S. Q. He, J. Song, J. L. Qu and Z. Cheng, *Chem. Soc. Rev.*, 2018, **47**, 4258.
47 S. J. Sun, L. N. Zhao, D. Wu, H. X. Zhang, H. C. Lian, X. L. Zhao, A. G. Wu and L. Y. Zeng, *ACS Appl. Bio Mater*, 2021, **4**, 1969.
48 H. M. Chen, Y. W. Qiu, D. D. Ding, H. R. Lin, W. J. Sun, G. D. Wang, W. C. Huang, W. Z. Zhang, D. Lee, G. Liu, J. Xie and X. Y. Chen, *Adv. Mater.*, 2018, e1802748.
49 B. S. Tian, S. K. Liu, L. L. Feng, S. H. Liu, S. L. Gai, Y. L. Dai, L. S. Xie, B. Liu, P. P. Yang and Y. L. Zhao, *Adv. Funct. Mater.*, 2021, **31**, 2100549.
50 M. Zhang, T. Zheng, B. L. Sheng, F. Wu, Q. C. Zhang, W. T. Wang, J. Shen, N. L. Zhou and Y. Sun, *Chem. Eng. J.*, 2019, **373**, 1054.
51 T. Y. Luo, Y. Nie, J. Lu, Q. J. Bi, Z. Y. Cai, X. Song, H. Ai and R. R. Jin, *Mater. Des.*, 2021, **208**, 109878.
52 (*a*) W. Sun, X. Z. Zhao, J. L. Fan, J. J. Du and X. J. Peng, *Small*, 2019, **15**, 1804927; (*b*) T. Liu, H. J. Wu, Y. Liang, X. J. Liang, H. C. Huang, Y. Z. Zhao, Q. C. Liao, Y. Q. Chen, A. M. Leng, W. J. Yuan, G. Y. Zhang, J. Peng and Y. H. Chen, *World J. Gastroenterol.*, 2016, **22**, 5342.
53 (*a*) M. H. Park, J. G. E. J. Kim, J. S. Jung and H. Hyun, *Chem. Commun.*, 2020, **56**, 4180; (*b*) Q. Y. Zheng, X. M. Liu, Y. F. Zheng, K. W. K. Yeung, Z. D. Cui, Y. Q. Liang, Z. Y. Li, X. B. Wang and S. L. Wu, *Chem. Soc. Rev.*, 2021, **50**, 5086.
54 A. Nasrin, M. Hassan and V. G. Gomes, *Nanoscale*, 2020, **12**, 20598.
55 S. Z. Yi, S. M. Deng, X. L. Guo, C. C. Pang, Ji. Y. Zeng, S. C. Ji, H. Liang, X. C. Shen and B. P. Jiang, *Carbon*, 2021, **182**, 155.
56 (*a*) X. Y. Deng, Z. W. Shao and Y. L. Zhao, *Adv. Sci.*, 2021, **8**, 2002504; (*b*) X. P. Duan, C. Chan and W. B. Lin, *Angew. Chem., Int. Ed.*, 2019, **58**, 670.
57 M. Jiao, Y. X. Wang, W. J. Wang, X. Y. Zhou, J. Xu, Y. J. Xing, L. Chen, Y. Y. Zhang, M. H. Chen, K. Xu and S. H. Zheng, *Chem. Eng. J.*, 2022, **440**, 135965.
58 H. Wang, Q. X. Mu, K. Wang, R. A. Revia, C. Yen, X. Y. Gu, B. W. Tian, J. Liu and M. Q. Zhang, *Appl. Mater. Today*, 2019, **14**, 108.
59 Y. Han, H. M. Liu, M. Fan, S. T. Gao, D. H. Fan, Z. G. Wang, J. Chang, J. C. Zhang and K. Ge, *J. Colloid Interface Sci.*, 2022, **616**, 595.
60 (*a*) Y. Zhang, X. Q. Zhang, H. C. Yang, L. Yu, Y. J. Xu, A. Sharma, P. Yin, X. Y. Li, J. S. Kim and Y. Sun, *Chem. Soc. Rev.*, 2021, **50**, 11227; (*b*) W. J. Ren, H. Q. Wang, Q. Chang, N. Li, J. L. Yang and S. L. Hu, *Carbon*, 2021, **184**, 102; (*c*) N. Tao, H. H. Li, L. Deng, S. F. Zhao, J. Ouyang, M. Wen, W. S. Chen, K. Zeng, C. W. Wei and Y. N. Liu, *ACS Nano*, 2022, **16**, 485.
61 B. J. Geng, S. Xu, P. Li, X. K. Li, F. L. Fang, D. Y. Pan and L. X. Shen, *Small*, 2022, **18**, 2103528.
62 B. J. Geng, J. Y. Hu, Y. Li, S. N. Feng, D. Y. Pan and L. X. Shen, *Nat. Commun.*, 2022, **13**, 5735.
63 H. Wang, X. C. Liu, X. Y. Yan, J. W. Fan, D. W. Li, J. S. Ren and X. G. Qu, *Chem. Sci.*, 2022, **13**, 6704.
64 (*a*) Z. M. Huang, P. P. Yu and J. H. Tang, *OncoTargets Ther.*, 2020, **13**, 5395; (*b*) B. H. Wang, J. Shen, Z. X. Wang, J. X. Liu, Z. F. Ning and M. C. Hu, *J. Breast Cancer*, 2018, **21**, 11; (*c*) K. Hu, J. Zhang, M. Yu and C. E. Xiong, *Future Oncol.*, 2016, **13**, 1479.
65 H. Wang, K. Wang, B. W. Tian, R. Revia, Q. X. Mu, M. Jeon, F. C. Chang and M. Q. Zhang, *Small*, 2016, **12**, 6388.

66 Y. L. Bai, J. J. Zhao, S. L. Wang, T. R. Lin, F. G. Ye and S. L. Zhao, *ACS Appl. Mater. Interfaces*, 2021, **13**, 35365.
67 Y. L. Bai, J. J. Zhao, L. L. Zhang, S. L. Wang, J. Hua, S. L. Zhao and H. Liang, *Adv. Healthcare Mater.*, 2022, **11**, 2102759.
68 S. Sun, J. Q. Chen, K. Jiang, Z. D. Tang, Y. H. Wang, Z. J. Li, C. B. Liu, A. G. Wu and H. W. Lin, *ACS Appl. Mater. Interfaces*, 2019, **11**, 5791.
69 Y. Wang, K. Y. Wang, J. F. Zhao, X. G. Liu, J. Bu, X. Y. Yan and R. Q. Huang, *J. Am. Chem. Soc.*, 2013, **135**, 4799.
70 J. L. Liang, J. J. Liu, X. K. Jin, S. T. Yao, B. L. Chen, Q. W. Huang, J. H. Hu, J. M. Wan, Z. W. Hu and B. Wang, *ACS Appl. Bio Mater.*, 2020, **3**, 7122.
71 W. J. Liu, H. Gu, B. Ran, W. K. Liu, W. Sun, D. P. Wang, J. J. Du, J. L. Fan and X. J. Peng, *Sci. China Mater.*, 2022, **65**, 845.
72 M. Z. Yu, X. Z. Guo, H. J. Lu, P. L. Li, R. B. Huang, C. N. Xu, X. D. Gong, Y. H. Xiao and X. D. Xing, *Carbon*, 2022, **199**, 395.
73 B. Huang, X. M. Liu, Z. Y. Li, Y. F. Zheng, K. W. K. Yeung, Z. D. Cui, Y. Q. Liang, S. L. Zhu and S. L. Wu, *Chem. Eng. J.*, 2021, **414**, 128805.
74 M. Liu, L. Huang, X. Y. Xu, X. M. Wei, X. F. Yang, X. L. Li, B. N. Wang, Y. Xu, L. H. Li and Z. M. Yang, *ACS Nano*, 2022, **16**, 9479.
75 Y. Dong, H. Pang, H. Yang, C. Guo, J. Shao, Y. Chi, C. Li and T. Yu, *Angew. Chem.*, 2013, **125**, 7954.
76 X. Zheng, A. Ananthanarayanan, K. Luo and P. Chen, *Small*, 2015, **11**, 1620.
77 W. Wei, C. Xu, L. Wu, J. Wang, J. Ren and X. Qu, *Sci. Rep.*, 2014, **4**, 3564.
78 Y. Dong, H. Pang, H. Yang, C. Guo, J. Shao, Y. Chi, C. Li and T. Yu, *Angew. Chem., Int. Ed.*, 2013, **52**, 7800.
79 Z. Qian, X. Shan, L. Chai, J. Ma, J. Chen and H. Feng, *ACS Appl. Mater. Interfaces*, 2014, **6**, 6797.
80 J. Zhou, X. Shan, J. Ma, Y. Gu, Z. Qian, J. Chen and H. Feng, *RSC Adv.*, 2014, **4**, 5465.
81 J. F. Ma, L. Z. Zhang, X. Chen, R. G. Su, Q. Shi, S. Q. Zhao, Q. Xu and C. M. Xu, *Chin. Chem. Lett.*, 2020, **32**, 1532.
82 J. Wang, C. F. Wang and S. Chen, *Angew. Chem., Int. Ed.*, 2012, **51**, 9297.
83 S. Y. Park, H. U. Lee, E. S. Park, S. C. Lee, J. W. Lee, S. W. Jeong, C. H. Kim, Y. C. Lee, Y. S. Huh and J. Lee, *ACS Appl. Mater. Interfaces*, 2014, **6**, 3365.
84 H. Q. Song, X. J. Liu, B. Y. Wang, Z. Y. Tang and S. Y. Lu, *Sci. Bull.*, 2019, **64**, 1788.
85 M. Y. Li, C. Yu, C. Hu, W. B. Yang, C. T. Zhao, S. Wang, M. D. Zhang, Ji. Z. Zhao, X. N. Wang and J. S. Qiu, *Chem. Eng. J.*, 2017, **320**, 570.
86 W. D. Li, Y. Liu, B. Y. Wang, H. Q. Song, Z. Y. Liu, S. Y. Lu and B. Yang, *Chin. Chem. Lett.*, 2019, **30**, 2323.
87 (*a*) Y. L. Xu, C. L. Li, J. S. An, X. Ma, J. F. Yang, L. S. Luo, Y. Deng, J. S. Kim and Y. Sun, *Sci. China: Chem.*, 2023, **66**, 155; (*b*) Y. L. Xu, C. L. Li, X. Ma, W. Tuo, L. Tu, X. P. Li, Y. Sun, P. J. Stang and Y. Sun, *Proc. Natl. Acad. Sci. U. S. A.*, 2022, **119**, e2209904119; (*c*) C. L. Li, Y. L. Xu, L. Tu, M. Choi, Y. F. Fan, X. Q. Chen, J. L. Sessler, J. S. Kim and Y. Sun, *Chem. Sci.*, 2022, **13**, 6541.